

Photofragmentation Dynamics of the Thiomethoxy Radical

Michael B. Pushkarsky, Brian E. Applegate, and Terry A. Miller

Laser Spectroscopy Facility

Department of Chemistry

The Ohio State University

120 W. 18th Avenue

Columbus Ohio 43210

(June 30, 2000)

Abstract

The radiative and non-radiative decay of the \tilde{A}^2E electronic state of the CH_3S radical has been investigated using a variety of experimental techniques. Lifetimes have been measured for a number of vibrational levels; these data have been analyzed along with similar results previously obtained for other methoxy radical family members, CH_3O , CD_3O , and CF_3S . It is concluded that the totality of the data is best described by a model which postulates mode-selective fragmentation into a methyl (or fluoromethyl) radical and a O or S atom. For CH_3S there appears a second non-radiative decay channel, possibly producing $\text{H}+\text{CH}_2\text{S}$.

I. INTRODUCTION

The CH_3S radical is a member of the methoxy family, which includes the methoxy radical CH_3O , itself, as well as CF_3O and CF_3S . Methoxy has been the subject of many studies, both theoretical¹⁻⁷ and experimental⁸⁻²⁷, as have CF_3S ^{20,28,29} and CF_3O ,^{29,30} albeit to a lesser extent. In recent studies^{20,31} by our group the photofragmentation dynamics of $\text{CH}(\text{D})_3\text{O}$

and CF_3S have been studied as a function of energy and vibrational mode composition. It has been shown that the rate of photofragmentation in the $\tilde{A}^2\text{A}_1$ state is highly correlated with the vibrational mode to which it is excited. Complementary experiments by Neumark^{21,22} and co-workers on $\text{CH}(\text{D})_3\text{O}$ provided additional information about the nature and energy content of the fragments produced.

The electronic structure and photodynamics of the methylthio radical also have been subjects of both theoretical^{7,32,33} and experimental studies³⁴. Recently Neumark³⁵ reported results on the photodissociation of the CH_3S radical using photofragment translational spectroscopy. In this paper we report the directly measured rates for the photofragmentation process in the CH_3S radical as a function of total energy content and the particular vibrational mode into which the energy is deposited, using a set of techniques including laser induced fluorescence (LIF), fluorescence temporal decay (FTD) and fluorescence depletion spectroscopy (FDS). Having collected an extensive set of data for $\text{CH}(\text{D})_3\text{O}$, CF_3S and CH_3S in the $\tilde{A}^2\text{A}_1$ state we discuss the effects of chemical substitution on the dissociation dynamics.

II. EXPERIMENTAL SECTION

A. LIF and FTD experiments

Though extensive data on both the laser induced fluorescence spectrum and natural lifetimes of fluorescing vibrational levels in CH_3S are available in the literature, both LIF and FTD experiments were performed as a prerequisite to FDS. The main reason for starting with LIF and FTD experiments is to optimize the production of CH_3S in the free jet and confirm both the LIF assignments and lifetimes.

The free jet expansion and most experimental considerations for this study have been presented previously¹¹ but will be briefly summarized here. The CH_3S radicals were formed by 248 nm photolysis of $(\text{CH}_3\text{S})_2$ (Aldrich 99%, no further purification) seeded in helium

carrier gas by a KrF excimer laser (Lumonics Excimer-500). The expansion was formed using a commercial pulsed nozzle (General Valve).

The fluorescence was collected with a lens and projected onto a photomultiplier tube. The signal from the photomultiplier was sent to a digital oscilloscope (LeCroy 9400) and then stored on a computer. All spectral frequency calibration was performed by scanning an Fe/Ne hollow cathode lamp while simultaneously collecting the LIF from CH₃S. The error limits in the frequency measurements are derived from the accuracy of the measurement of the line’s frequency and its line width. From calibration of multiple scans the estimated absolute accuracy of our frequency values is $\pm 0.5 \text{ cm}^{-1}$.

In the FTD experiment the probe laser was tuned to a particular rotational line of a given vibronic transition and the time resolved fluorescence decay was recorded. The fluorescence temporal decay was taken for several individually resolved rotational levels for each vibrational band. The temporal resolution was determined by the PMT and associated electronics and is estimated to be 35 ns.

B. FDS Experiment

The setup of the FDS experiment has been described previously.^{20,31} Briefly the free jet expansion was crossed downstream from the nozzle with a “probe” laser (Hyperdye 300 Lumonics, 0.5 mJ/pulse, 0.15 cm^{-1} linewidth) beam for which the frequency was adjusted to excite a particular rotational level of a low-lying vibronic level (typically 3^2) of the \tilde{A} state. The fluorescence resulting from this laser was monitored. A second “depletion” laser (frequency doubled output of PDL2 Quanta Ray, 2 mJ/pulse, 0.3 cm^{-1} linewidth) beam was set counter propagating along the probe laser direction and its frequency scanned over the region of interest. When the depletion laser frequency is scanned over a transition terminating on a photofragmenting level of the molecule and originating from the same rovibronic level as the transition excited by the probe laser, the fluorescence from the probe laser decreases due to loss of population of the lower level by excitation and subsequent

dissociation.

An improved signal to noise ratio was achieved in the FDS experiments by splitting the probe beam and sending it through the expansion at two symmetrical locations with the free jet and only overlapping one of the beams with the depletion beam. If the fluorescence from each of the two probe beams is detected separately, the beam that is not overlapped with the depletion beam can be used as a reference to normalize shot-to-shot fluctuations in the fluorescence resulting from variations in the photolysis and probe lasers as well as the free jet expansion. To monitor separately LIF signals from two regions of the expansion with two PMTs a special optical set up is required. We used two lenses to focus the light sources from the two sides of the expansion onto the plane where a quartz prism was placed such that its lower edge was located between the two images. This arrangement allows the lower image to be propagated forward and reach PMT1 while the upper image was directed to PMT2.

The delay between depletion and probe lasers was set at 50 ns. The two LIF time resolved waveforms from PMT1 and PMT2 were recorded by the two channels of a digital scope and transferred to a PC through a GPIB interface using LabView 4.0 software. The ratio of the two integrated areas of the fluorescence temporal decays plotted vs. the frequency of the depletion laser constitutes the FDS spectrum.

III. RESULTS

A. Vibrational Assignment in the \tilde{A}^2A_1 Electronic State of CH_3S Radical

The CH_3S radical has three symmetric a_1 modes ν_1 , ν_2 , and ν_3 corresponding approximately to the C-H stretch, the umbrella bend of the methyl group, and the C-S stretch respectively and three asymmetric doubly degenerate e modes ν_4 , ν_5 , and ν_6 , corresponding approximately to the asymmetric C-H stretch, an H-C-H scissors motion, and a methyl-S rock. Its ground electronic state, \tilde{X}^2E , is subject to spin-orbit coupling that splits the vi-

brationless level 0_0 into two spin-orbit components separated by 259 cm^{-1} with the lower component being the $\omega = 3/2$ spin state. Because of the large spin-orbit splitting one would not expect that the $\omega = 1/2$ spin state to be populated in the free jet conditions; however it has been observed by different groups^{36,37} that transitions originating from this level have significant intensity due to incomplete cooling. In the present work we also observed these transitions in LIF; however we do not incorporate them in our analysis since they do not provide additional information about the \tilde{A}^2A_1 excited state. For this reason we give relative frequencies of all observed bands relative to the frequency of the $\omega = 3/2$ spin component of the origin band at 26526 cm^{-1} keeping in mind that the position of the true electronic origin (near the center of the spin-orbit components) is shifted to the red by $\approx 129.5\text{ cm}^{-1}$.

1. LIF spectrum

The vibrational structure up to 1500 cm^{-1} above the origin of the first excited electronic state of the CH_3S radical has been previously characterized by LIF spectroscopy³⁶⁻⁴⁰. Lee *et al.*³⁷ reported a free jet-cooled LIF spectrum in the region from 26200 cm^{-1} to 28570 cm^{-1} . The two observed strong progressions have been assigned as $3_0^n(\tilde{A}^2A_1 \leftarrow \tilde{X}^2E_{3/2})$, $n = 0..3$ and $2_0^1 3_0^n(\tilde{A}^2A_1 \leftarrow \tilde{X}^2E_{3/2})$, $n = 0$ and 1 . The transitions in several weaker progressions have been assigned as hot bands. No transitions to excitations of ν_1 , the symmetric C-H stretch, have been observed, most likely due to unfavorable Frank-Condon factors. All of the progressions become weak at frequencies above 27320 cm^{-1} and completely disappear above 28016 cm^{-1} .

The transitions from the ground electronic state origin to asymmetric vibrations ν_4 , ν_5 , and ν_6 in the \tilde{A}^2A_1 state are allowed only as a result of Jahn-Teller activity in the \tilde{X}^2E state. All of the members of the methoxy family are subject to Jahn-Teller distortions; however CH_3S exhibits the weakest Jahn-Teller effect in the group. In accordance with this fact no asymmetric vibrations were observed in the LIF spectrum with the exception of one weak feature at 27161.5 cm^{-1} which was assigned as 6_0^1 ($\omega = 3/2$). We have reproduced a large

portion of the LIF spectrum and confirmed frequencies and assignments reported by Lee *et al.* (Table I).

2. Dark vibrational levels

For the FDS survey scans the probe laser was tuned to a strong resolved rovibronic transition in the center of the 3_0^2 band (labeled “1” in the Fig. 1(A)). The FDS spectrum was recorded in the range from 1500 cm^{-1} to 3000 cm^{-1} above the origin. The relative frequencies and vibrational assignments of the observed transitions are given in the Table I. The FDS spectrum is fairly simple with all observed features assignable to additional transitions in the progressions observed in LIF. The progression in 3^n has been observed in depletion for $n=3-7$. Likewise the other major progression seen in LIF, 2^13^m , has been observed in depletion for $m=2-5$. The highest frequency band observed at 29505 cm^{-1} (lifetime-broadened to $\approx 20\text{ cm}^{-1}$ FWHM) was assigned as 2^13^5 ; however, 3^8 is predicted (by extrapolation using the frequencies of the lower members in the progression) to be only 7 cm^{-1} higher in frequency. Thus there is a strong possibility that both bands are present with overlapping contours.

After survey scans were completed, the power of the depletion laser was decreased to avoid power saturation and short FDS scans were performed across each observed vibrational band with the probe laser being tuned first to the rovibronic transition labelled “1” and next at the transition labelled “2” (see Fig. 1A) both belonging to the 3_0^2 band. As the lines “1” and “2” correspond to the rotational transitions involving different K_a levels ($K_a'' = -1 \rightarrow K_a' = 0$ and $K_a'' = 0 \rightarrow K_a' = 1$ respectively) we were able to test the possibility of K_a' dependence of the lifetime-broadening in the range of accessible $K_a' = 0$ and 1. The FDS spectra become sufficiently lifetime-broadened to wash out rotational structure for 3^n , $n \geq 5$ and 2^13^m , $m \geq 4$ as illustrated in Fig. 1, which depicts FDS spectra for a number of bands from progression ν_3 . It should be noted that even in the case when the FDS spectrum is broadened K_a' selective lifetime measurement is possible. However, as Fig. 1B shows, there

is no observable K'_a -dependence for the lifetimes.

B. Lifetime measurements in the \tilde{A}^2A_1 State

We have measured (or bracketed) the natural lifetimes for all of the observed vibrational levels in the \tilde{A}^2A_1 electronic state. For the “bright” fluorescing vibrational levels the natural lifetimes were measured by the FTD technique. For “dark” levels we have employed the FDS technique and determined natural lifetimes by fitting the lifetime broadening of individual rotational levels.

1. Bright vibrational levels

Table I compares the lifetimes of the “bright” vibrational levels measured by the FTD technique in this work to those reported by Lee *et al.*. Our data is in the good agreement (Table I). The only exception to this statement is the weak and short-lived the 3^3 level, for which we report $\tau \leq 35$ ns, compared to previously reported 70(35) ns. It should be mentioned that we observed a weak, long-lifetime (260 ns) component in the fluorescence decay for this band, which we believe is due to collisional relaxation. It may be that this effect has lead to the discrepancy in the measured lifetime.

2. Dark vibrational levels

The lifetime broadening of the FDS features beyond the instrumental resolution provides a direct way to measure the natural lifetime. The following algorithm has been used to obtain lifetimes via measurements of the spectral broadening. First the FDS spectra of the three bands (3^4 , 2^13^2 , and 2^13^3) which do not show any measurable broadening and have virtually identical rotational structure (exemplified by the FDS spectrum of the 3^4 band in the Fig. 1B) were simulated using Gaussian lineshape functions. When transition “1” was probed the FDS spectra of each band consisted of a single line, which was simulated by a Gaussian

function with $\sigma_G = 0.32 \text{ cm}^{-1}$, related to the FWHM by the expression $2\sigma_G(\ln 4)^{1/2}$. When the probe laser was tuned to rotational transition “2” the FDS spectra consisted of one strong line and the two weak lines, each on either side. In the latter case three Gaussian functions with appropriate intensities and the same line width $\sigma_G = 0.32 \text{ cm}^{-1}$ were used. To simulate the lifetime broadened spectra the constructed lineshape functions were modified by replacing each Gaussian by a Voigt function with a variable Lorentzian width, σ_L , while keeping σ_G fixed at previously determined value. The parameter σ_L was fit to the profile of broadened features. The values of σ_L ($2\sigma_L = \text{FWHM}$) obtained from the fit were converted to lifetimes using the following relation⁴¹

$$\tau = 1/4\pi c\sigma_L \tag{1}$$

For every FDS feature at least three different experimental traces were fit.

As mentioned previously, no lifetime variations beyond experimental error were observed by alternating the frequency of the probe laser between transitions “1” and “2” indicating the lack of K'_a dependence in the photodissociation process (within our experimental error) for all observed dark vibrational levels.

For completeness the lifetimes determined by Neumark *et al.*³⁵ via the analysis of anisotropy of photofragment angular distribution, measured in their experiment were added in the Table I. The reported lifetimes are obviously a result of very indirect method, but it is interesting to compare them with our data. The lifetimes produced in that work are about an order of magnitude larger than those we obtained in our measurements. Such a discrepancy is not particularly surprising, taking into account the indirectness of the method.

IV. DISCUSSION

There are two complementary approaches to the experimental study of the photofragmentation: (i) the detection of the disappearance of the fragmenting molecules and (ii) detection of the appearance of the photofragments. In the present and a number of previous

papers^{31,42,20} we have utilized the first approach to study photofragmentation in the \tilde{A}^2A_1 excited electronic state of four members (CH_3O , CD_3O , CF_3S , and CH_3S) of the methoxy family. For these radicals (with the exception of CF_3S) there exist complementary results obtained via the photofragment translational spectroscopy^{21,22,35} that permits the detection of the photofragments (sulfur atoms and methyl radicals in case of CH_3S radical). In order to discuss the present results for CH_3S it is important to briefly review earlier observations for $\text{CH}(\text{D})_3\text{O}$ and CF_3S and compare them with the present results for CH_3S .

If one assumes that the vibrationless level decays at the radiative lifetime and therefore corresponds to a fluorescence quantum yield of 1, the ratio $\frac{\tau_{\nu'}}{\tau_0}$ is then the effective quantum yield of the emission from level ν' . We show in Fig. 2 plots of $\log \frac{\tau_{\nu'}}{\tau_0}$ vs vibrational energy for all four molecules for the transitions terminating in the various excited vibrational levels. The following four paragraphs briefly summarize the information in the plots of Fig. 2:

(i) In CH_3O ^{19,20} the normal modes ν_2 and ν_3 are mixed by Fermi resonance. As a result of such mixing if a molecule is excited to a given combination of ν_2 and ν_3 it will rapidly oscillate between the umbrella bend (ν_2) and the C-O stretch (ν_3). Such a fast randomization of energy should preclude mode selectivity in the photofragmentation as the normal mode description is no longer valid. In accordance with this picture we see in methoxy a progression that has a threshold for photofragmentation between $m = 5$ and 6 in the Fermi multiplet, $(\nu_2 + \nu_3)^m$, while all members of the Fermi multiplet (depicted by a single point on the Fig. 2) for a given m have the same lifetime within experimental accuracy. However the two other shown progressions involving combinations with asymmetric vibrational modes ν_4 and ν_5 demonstrate that in the absence of Fermi resonance, mode selective behavior occurs.

(ii) In CD_3O ³¹ the fragmentation threshold is observed between 5 and 6 quanta of ν_3 in pure ν_3 progression, similar to that in methoxy. However the lifted Fermi resonance between ν_2 and ν_3 allows for mode selectivity in the fragmentation process manifested by the fact that the threshold for photofragmentation in pure ν_3 and combinations $\nu_2 + \nu_3$ occur not at the same total energy but at the same number of quanta of ν_3 , clearly implying

that the ν_3 mode primarily promotes photofragmentation. For completeness two additional progressions, involving asymmetric vibrational modes are added and further illustrate the mode selectivity.

(iii) In the LIF/FDS spectrum of CF_3S^{43} all three symmetric modes and their numerous combinations are observed. The non-radiative process is, apparently, very mode-selective with the ν_3 mode being the most active with the threshold between $n=3$ and $n=4$ for the pure 3^n progression. Other combination progressions involving 3^n tend to have a threshold at $n=2$ to 3 , while progressions not involving ν_3 , for practical purposes, do not dissociate.

(iv) The plot for CH_3S is generated from the data in the Table I and shows a pattern somewhat different from the three described above. First of all, the 3^n progression has a threshold between 3^1 and 3^2 while the $2^1 3^n$ progression has a threshold between $n=0$ and 1 , thus indicating significant contributions from ν_2 in promoting photodissociation. Secondly one may note that in case of CH_3S the natural lifetimes steadily drop from 1130 ns for the origin to 860 ns for 3^1 and 460 ns for 2^1 before nose-diving after the addition of a subsequent quantum of ν_3 while for other family members the lifetimes for all vibronic levels are practically constant (on the scale shown) from the origin until reaching the first vibrational level above the fragmentation threshold.

We have previously shown³¹ that one can usefully plot (see Fig. 3) the quantum yields vs the extension of the C–Y(Y=O or S) bond length. The bond length is deduced from *ab initio* calculations at the RHF/6-31G* level which yield the classical turning point and are scaled as a function of the normal mode excitation, ν_i . These values are given in Table II.

Such a representation is useful because as Fig. 3 shows that unlike when plotted against energy, all the observed vibrational levels roughly fall on a single curve when quantum yield is plotted against bond extension. This behavior can be rationalized by the fact that for all the methoxy family radicals the \tilde{A}^2A_1 electronic state correlating asymptotically to $\text{CH}_3(\tilde{X}^2A_2'')+\text{S}(^1\text{D})$ products is crossed by the three repulsive surfaces ^4E , 2A_2 , and 4A_2 correlating to the ground state products $\text{CH}_3(\tilde{X}^2A_2'')+\text{S}(^3\text{P})$. The repulsive states are coupled to the \tilde{A}^2A_1 electronic state in the vicinity of their intersection seams and this coupling

is responsible for the non-adiabatic (predissociative) photofragmentation. A molecule photoexcited into a given vibrational level of the bound \tilde{A}^2A_1 state in sampling its PES crosses a seam of intersection with the repulsive state with a probability to “hop” to the repulsive curve and proceed to fragmentation, leading to O(S) and CH(F)₃ radical in the ground electronic state. In this picture the observed vibrational selectivity for CH(D)₃O and CF₃S is a reflection of the fact that different normal modes correspond to motions sampling different regions of the PES of the \tilde{A}^2A_1 state. The model also implies a lack of communication (mixing) between the various vibrational modes, contrary to the conventional wisdom, suggesting that in molecules of this size the internal energy will be rapidly redistributed statistically⁴⁴. The lowest energy point on the seam may be considered as the “transition state” for fragmentation, and the internal coordinate connecting the minimum of the PES of the \tilde{A}^2A_1 state to this “transition state” may be considered the “reaction coordinate”. The experimental data on CD₃O and CF₃S clearly show that the normal mode ν_3 associated with the C-Y (Y = O or S) stretch internal coordinate appears to promote the fragmentation most efficiently while ν_2 (the umbrella bend) appears to be ineffective in promoting fragmentation. This implies that for these molecules, the reaction coordinate should lie primarily along the C-Y stretch.

The corresponding plot for the CF₃S radical shows a very similar picture to that of CD₃O. Again, regardless of the mode composition of the individual vibrational levels, a common fragmentation threshold at the value of C-S extension ≈ 0.25 Å is observed. Consequently, the C-S internal coordinate well approximates the “reaction coordinate” for the photofragmentation reaction in the CF₃S radical. A couple of outliers on this plot correspond to high frequency bands. They indicate the limitations of the proposed model at higher excitation energies, where higher order mixing mechanisms begin to become important.

The corresponding plot for CH₃S reveals a picture significantly different from those obtained for other family members. The data points on the plot do not form a single curve allowing one to determine a unique minimal C-S extension required to initiate fragmentation. Instead one can see two clearly distinguishable curves, formed by points from the two

observed progressions, 3^n and 2^13^n . The lower curve belonging to bands terminating in combinations 2^13^n , appear to fragment at shorter C-S extensions than those of the higher curve representing pure overtones 3^n (at the same n). It appears that the C-S extension is not a measure of whether CH_3S undergoes photofragmentation. Therefore one concludes that the model that successfully explains mode selective photofragmentation in CH_3O , CD_3O , and CF_3S radicals does not work nearly so well for the CH_3S radical.

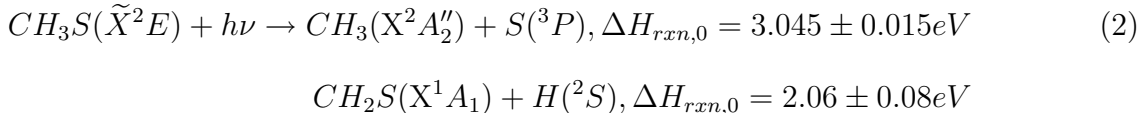
To try to understand this apparent failure, it is good to examine the three independent physical assumptions upon which the model is built: (i) the existence of a single dominant nonradiative channel (coupling to the lowest of the three repulsive electronic state, leading to the methyl radical and S atom), (ii) increase of C-O(S) internal coordinate being the only geometry change required to reach the “transition state” located on the intersection seam with the repulsive state, and (iii) lack of mixing between vibrational modes. We note that the breakdown of either assumption (ii) or (iii) (or both) would still make fragmentation into CH_3 and S atom the only major non-radiative channel, because regardless of the details of the dynamics, as the molecule reaches the seam, the repulsive character of the perturbing electronic state would lead to a single set of dissociation products. On the other hand the invalidation of assumption (i) implies that the \tilde{A}^2A_1 excited state of CH_3S is subject to more than one non-radiative process yielding different photofragments. In this case the observed natural lifetime dependence vs. vibrational excitation is a manifestation of a competition between processes.

The data from our experiments alone do not permit us to distinguish between mechanisms (i)-(iii) because no information about dissociation products is provided. However the results of the recent photofragment translational spectroscopy study³⁵ complement our results by providing an action spectrum of the $\text{S}+\text{CH}_3$ photofragmentation channel in the region from 2700 to 32000 cm^{-1} as shown on Fig 4. One can see that, while the spectrum is congested due to the higher rotational temperature and transitions originating from the populated upper spin-orbit component, the spectral structure is still easily assigned to two progressions, 3^n and 2^13^n . The remarkable feature of this spectrum is that the progression 2^13^n starts from

$n=3$, thereby indicating that the excitation of vibrational levels 2^13^1 and 2^13^2 do not lead to fragmentation to sulfur atom and methyl radical. Moreover, the authors specifically remarked that an extensive effort was made to observe the latter two transitions in the action spectrum, but without success. Likewise, though the 3^2 level has been reported as the lowest energy level dissociating into CH_3+S , the published action spectrum (Fig. 4) shows low intensity for the 3^2 band, indicating that only a small fraction of the excited molecules actually result in CH_3+S products. Thus the action spectrum alone shows generally a picture of mode-selective fragmentation into CH_3+S , with ν_3 being the promoting vibration with the fragmentation threshold at the three quanta of ν_3 .

On the other hand, in our experiments we observed the 3^2 and 2^13^1 bands in LIF with short lifetimes of 250 ns and 60 ns respectively, while 2^13^2 band was observed only in FDS spectrum, and hence, is completely dark. The comparison of the natural lifetimes of these two levels with that of the origin shows that over 80%, 94% and 99% of molecules excited into 3^2 , 2^13^1 and 2^13^2 levels respectively, undergo some kind of a non-radiative process. As this process is not fragmentation into methyl radical and sulfur atom, it must lead to some other set of photoproducts.

Thermodynamically accessible dissociative pathways for the methylthio radical for excitation energies in the vicinity of the vibrationless level of $\tilde{A}^2\text{A}_1-\tilde{X}^2\text{E}$ transition are³⁵



Consequently, for the explored excitation energies, a second non-radiative channel is the fragmentation of CH_3S into $\text{CH}_2\text{S}+\text{H}$, likely via internal conversion from the $\tilde{A}^2\text{A}_1$ state to highly vibrationally excited levels of the $\tilde{X}^2\text{E}$ state.

The conclusion that more than one nonradiative channel is present in the $\tilde{A}^2\text{A}_1$ state of the CH_3S radical so far is based upon a negative experimental result i.e. the absence of the three short-lived vibrational features in the action spectrum. However additional evidence in favor of the existence of another channel comes from the comparison of the natural lifetimes

of the vibrationless and lowest energy vibrational levels of the CH₃S radical with the rest of methoxy family. Fig. 2 shows that in CH₃O, CD₃O, and CF₃S radicals there is a clear energy threshold for a photofragmentation process, and all the vibrational levels with energies lower than the threshold value have natural lifetimes, practically coinciding with that of the vibrationless level. To the contrary in the CH₃S radical there is no clear energy threshold for fragmentation. Instead one can see a steady decrease in the lifetimes of the vibrational levels. This observation is consistent with the existence of a non-radiative channel even at the lowest vibrational excitations. Moreover even the lifetime of the vibrationless level of the CH₃S radical (1130ns) is more than two times shorter than those for the other radicals in the family (2800 ns, 2900 ns, and 2740 ns, for CH₃O, CD₃O, and CF₃S respectively) while the ν^3 factor in the Einstein A coefficient suggests that it should have the longest radiative lifetime in the family. Therefore even the vibrationless level of the \tilde{A}^2A_1 state of the methylthio radical is likely subject to a non-radiative process.

Summarizing these observations one can construct a picture of the photodissociation dynamics in the \tilde{A}^2A_1 electronic state of the CH₃S radical, consistent with all the experimental observations. Upon photoexcitation into \tilde{A}^2A_1 state the thiomethoxy radical undergoes two different non-radiative processes. One is the coupling to the lowest of the three repulsive electronic states, yielding CH₃+S products. This channel, dominating for the vibrational excitations involving more than two quanta of ν_3 , is mode selective with the ν_3 mode being the promoting vibration similar to the rest of the methoxy family. However in the vicinity of the minimum of the PES of the \tilde{A}^2A_1 electronic state, i.e., the region sampled by the molecule excited with less than 3 quanta of ν_3 , a second non-radiative process, likely internal conversion, followed by dissociation into CH₂S+H, is dominant. Clearly, experiments aiming at the detection of H or CH₂S fragments would be useful to directly establish the existence of this channel. Unfortunately the photofragmentation experiments are insensitive³⁵ to the H loss channel, so other experimental approaches would be required.

Before concluding we also note that our data allows us to study the effect of substitution of sulfur for oxygen on the photofragmentation process. It appears that S substitution

makes the most pronounced effect on the magnitude of the non-adiabatic coupling between the \tilde{A}^2A_1 and the repulsive electronic states. As one can see from Fig. 3 for all the studied radicals the vibrational levels with the C-O(S) extensions well exceeding the fragmentation threshold, value have nearly constant fragmentation rates. For both sulfur containing radicals these values are of the order of 1ps, while for both protonated and deuterated methoxy radicals they are estimated to be $\tau \geq 20$ ps. Thus the ratio of the photofragmentation rates of the sulfur and oxygen-containing radicals is a factor of 20 or higher. This result qualitatively agrees with the recent *ab initio* calculations⁷, which predicted spin-orbit coupling matrix elements between \tilde{A}^2A_1 and the lowest repulsive state, 4A_2 , to be 25 cm⁻¹, 75 cm⁻¹, and 88 cm⁻¹ for CH₃O, CH₃S, and CF₃S respectively (note that the fragmentation rate should be proportional to the square of the coupling matrix element). Hence roughly an order of magnitude shorter lifetime for the photofragmentation process should be expected for the S-containing radicals, as is observed.

V. CONCLUSIONS

We have measured the natural lifetimes for a number of “dark” predissociating vibrational levels in the CH₃S radical. We have applied a simple model to explain mode selectivity in the CH₃S radical as well as previously studied methoxy radicals, CH(D)₃O and CF₃S. While this model is suitable for explanation of the mode selectivity of the other radicals, it fails in the case of the CH₃S. However, by comparing our data with complementary photofragment action spectra, we can explain all the experimental data by assuming that in addition to a vibrational mode-selective photofragmentation channel leading to a sulfur atom and methyl radical, there exists another non-radiative channel, likely internal conversion into the ground state followed by fragmentation to H and CH₂S.

VI. ACKNOWLEDGMENTS

The authors acknowledge the support of this work by the National Science Foundation via grant 9974404. We thank Dr. T. Barckholtz for performing the *ab initio* calculations.

REFERENCES

- ¹ D. R. Yarkony, I. Schaefer, H. F., and S. Rothenberg, *J. Am. Chem. Soc.* **96**, 656 (1974).
- ² D. Ohkubo, T. Fujita, and H. Sato, *J. Mol. Struct.* **36**, 101 (1977).
- ³ G. D. Bent, G. F. Adams, R. H. Bartram, G. D. Purvis, and R. J. Bartlett, *J. Chem. Phys.* **76**, 4144 (1982).
- ⁴ S. Saebo, L. Radom, and I. H. F. Schaefer, *J. Chem. Phys.* **78**, 845 (1983).
- ⁵ C. F. Jackels, *J. Chem. Phys.* **76**, 505 (1982).
- ⁶ C. F. Jackels, *J. Chem. Phys.* **82**, 311 (1985).
- ⁷ Q. Cui and K. Morokuma, *Chem. Phys. Lett.* **263**, 54 (1996).
- ⁸ P. Misra, X. Zhu, C. Y. Hsueh, and J. B. Halpern, *Chem. Phys.* **178**, 377 (1993).
- ⁹ P. Misra and X. Zhu, *Spectros. Lett.* **26**, 389 (1993).
- ¹⁰ P. Misra, X. Zhu, and A. Nur, *Spectros. Lett.* **25**, 639 (1992).
- ¹¹ S. C. Foster, P. Misra, T.-Y. Lin, C. P. Damo, C. C. Carter, and T. A. Miller, *J. Phys. Chem.* **92**, 5914 (1988).
- ¹² X. Liu, C. P. Damo, T.-Y. Lin, S. C. Foster, P. Misra, L. Yu, and T. A. Miller, *J. Phys. Chem.* **93**, 2266 (1989).
- ¹³ N. L. Garland and D. R. Crosley, *J. Phys. Chem.* **92**, 5322 (1988).
- ¹⁴ K. Fuke, K. Ozawa, and K. Kaya, *Chem. Phys. Lett.* **126**, 119 (1986).
- ¹⁵ D. E. Powers, J. B. Hopkins, and R. E. Smalley, *J. Phys. Chem.* **85**, 2711 (1981).
- ¹⁶ G. Inoue, H. Akimoto, and M. Okuda, *Chem. Phys. Lett.* **63**, 213 (1979).
- ¹⁷ G. Inoue, H. Akimoto, and O. M., *J. Chem. Phys.* **72**, 1769 (1980).
- ¹⁸ Y. Y. Lee, G. H. Wann, and Y. P. Lee, *J. Chem. Phys.* **99**, 9465 (1993).

- ¹⁹ D. E. Powers, M. Pushkarsky, and T. A. Miller, *J. Chem. Phys.* **106**, 6863 (1997).
- ²⁰ D. E. Powers, M. Pushkarsky, and T. A. Miller, *J. Chem. Phys.* **106**, 6878 (1997).
- ²¹ D. L. Osborn, D. J. Leahy, and D. Neumark, *Chem. Phys. Lett.* **235**, 484 (1995).
- ²² D. L. Osborn, D. J. Leahy, and D. Neumark, *J. Phys. Chem. A* **101**, 6583 (1997).
- ²³ A. Geers, J. Kappert, F. Temps, and J. W. Wiebrecht, *J. Chem. Phys.* **101**, 3618 (1994).
- ²⁴ S. Dertinger, A. Geers, J. Kappert, J. Wiebrecht, and F. Temps, *Faraday Discuss.* **102**, 31 (1996).
- ²⁵ S. Y. Chiang, Y. C. Hsu, and Y. P. Lee, *J. Chem. Phys.* **90**, 81 (1989).
- ²⁶ S. D. Brossard, P. G. Carrick, E. L. Chappell, S. C. Hulegaard, and P. C. Engelking, *J. Chem. Phys.* **84**, 2459 (1986).
- ²⁷ T. Ebata, H. Yanagishita, K. Obi, and I. Tanaka, *Chem. Phys.* **69**, 27 (1982).
- ²⁸ R. R. Wright and T. A. Miller, *J. Mol. Spectros.* **194**, 219 (1999).
- ²⁹ T. A. Barckholtz, M.-C. Yang, and T. A. Miller, *Mol. Phys.* **97**, 239 (1999).
- ³⁰ M.-C. Yang, J. M. Williamson, and T. A. Miller, *J. Mol. Spectros.* **186**, 1 (1997).
- ³¹ B. E. Applegate, M. B. Pushkarsky, and T. A. Miller, *J. Phys. Chem.* **103**, 1538 (1999).
- ³² C. W. Hsu, C. L. Liao, Z. X. Ma, P. J. H. Tjossem, and C. Y. Ng, *J. Chem. Phys.* (1992).
- ³³ T. Barckholtz and T. A. Miller, *Int'l. Rev. of Phys. Chem.* **17**, 435 (1998).
- ³⁴ S. H. Wilson, M. N. Ashfold, and R. N. Dixon, *J. Chem. Phys.* (1994).
- ³⁵ R. T. Bise, H. Choi, H. B. Pedersen, D. H. Mordaunt, and D. M. Neumark, *J. Chem. Phys.* **110**, 808 (1999).
- ³⁶ X. Liu, Y.-C. Hsu, and T. A. Miller, *J. Chem. Phys.* **90**, 6852 (1989).

- ³⁷ S.-Y. Chiang and Y.-P. Lee, *J. Chem. Phys.* **95**, 66 (1991).
- ³⁸ M. Suzuki, G. Inoue, and H. Akimoto, *J. Chem. Phys.* **81**, 5405 (1984).
- ³⁹ G. Black and L. E. Jusinski, *J. Chem. Soc., Faraday Trans.* **82**, 2143 (1986).
- ⁴⁰ G. Black and L. E. Jusinski, *J. Chem. Phys.* **85**, 5379 (1986).
- ⁴¹ W. Demtroder, *Laser Spectroscopy, Basic Concepts and Instrumentation* (Springer-Verlag: Berlin, Heidelberg, New York, 1982).
- ⁴² D. E. Powers, M. B. Pushkarsky, M.-C. Yang, and T. A. Miller, *J. Phys. Chem.* **101**, 9846 (1997).
- ⁴³ D. E. Powers, M. Pushkarsky, and T. A. Miller, *Chem. Phys. Letts.* **247**, 548 (1995).
- ⁴⁴ P. J. Robinson and K. A. Holbrook, *Unimolecular Reactions* (John Wiley, New York, 1972).

Figure Captions

1. **(A)** The LIF Spectrum of the 3^2 Band. Numbers “1” and “2” mark two rotational transitions, corresponding to $K'_a = 0$ and $K'_a = 1$ levels respectively, that have been probed while taking FDS spectra shown below.**(B)** The FDS spectra of the Three Members of 3^n Progression. The spectra shown in the left(right) column were taken with the probe laser being tuned to the transition “1”(“2”) of the 3^2 band. These spectra illustrate several points, including lifetime broadening, lack of K'_a selectivity in fragmentation, and the fact that the rotational structure of FDS spectrum depends upon the probed transition.
2. Plots of the Log of the Effective Quantum Yield (see text) vs. Energy (relative to the vibrationless level). The open symbols in the plots represent points for which the lifetimes can only be determined to lie between the limits, $20 \text{ nsec} < \tau < 20 \text{ psec}$. Within this range the vertical placement on the plot is arbitrary. The upper left plot shows the vibrational progressions in CH_3O where m equals the number of quanta of excitation into the Fermi multiplet $(\nu_2 + \nu_3)^m$. For these plots the energy and lifetimes of the Fermi multiplets were averaged to produce the points on the plots. The other plots show the corresponding vibrational progressions for CD_3O , CF_3S and CH_3S radicals where n equals the number of quanta of excitation into 3^n
3. Plots of the Log of the Effective Quantum Yield vs. R (R is the maximum C-O(S) extension – see text for details)..
4. Action spectrum of CH_3S adapted from Bise, *et al.*³⁵ monitoring the channel $\text{S}+\text{CH}_3$. The two vertical arrows point at the positions of the 2^13^1 and 2^13^2 bands, not observed in the action spectrum, but observed respectively in LIF with a significantly shortened lifetime, and in the FDS spectrum.

FIGURES

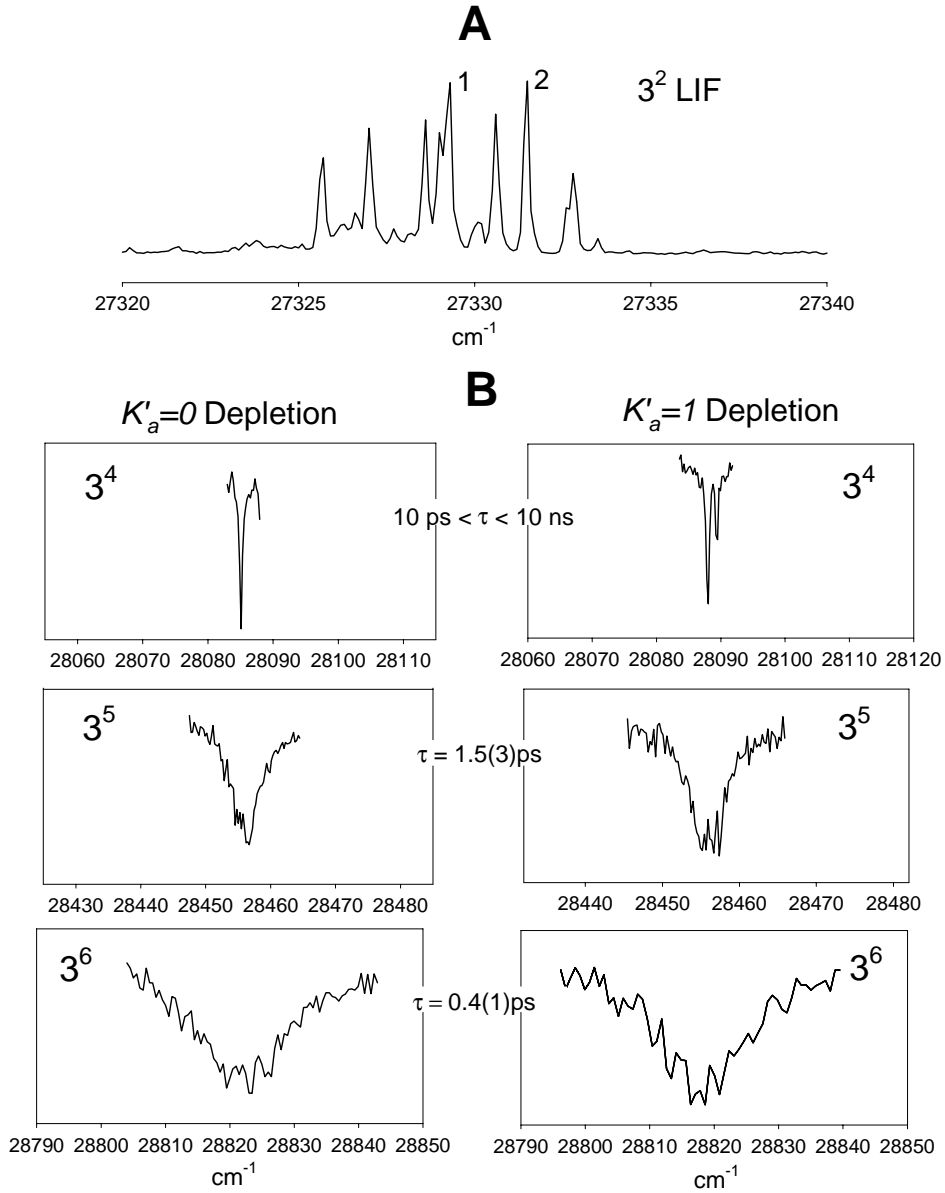


FIG. 1. (A) The LIF Spectrum of the 3^2 Band. Numbers “1” and “2” mark two rotational transitions, corresponding to $K'_a = 0$ and $K'_a = 1$ levels respectively, that have been probed while taking FDS spectra shown below. (B) The FDS spectra of the Three Members of 3^n Progression. The spectra shown in the left(right) column were taken with the probe laser being tuned to the transition “1”(“2”) of the 3^2 band. These spectra illustrate several points, including lifetime broadening, lack of K'_a selectivity in fragmentation, and the fact that the rotational structure of FDS spectrum depends upon the probed transition.

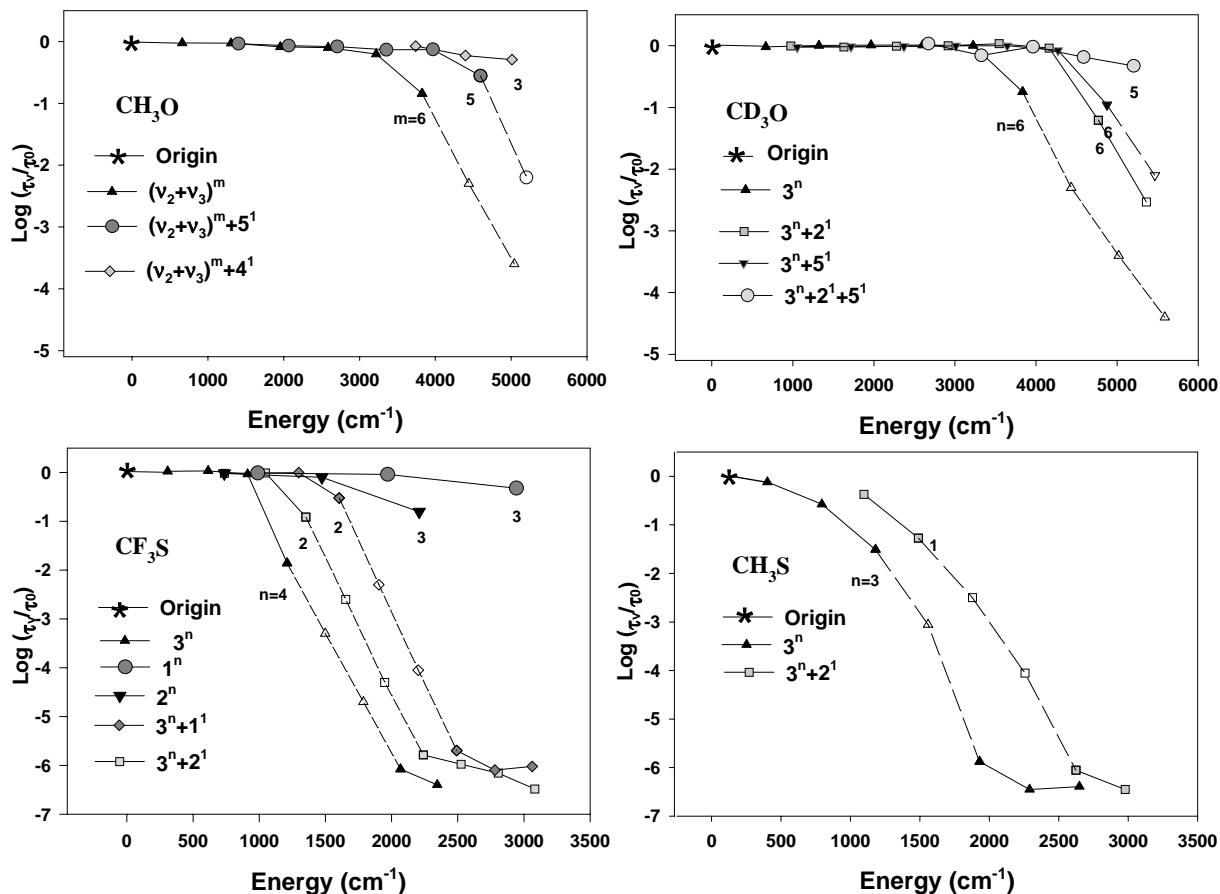


FIG. 2. Plots of the Log of the Effective Quantum Yield (see text) vs. Energy (relative to the vibrationless level). The open symbols in the plots represent points for which the lifetimes can only be determined to lie between the limits, $20 \text{ nsec} < \tau < 20 \text{ psec}$. Within this range the vertical placement on the plot is arbitrary. The upper left plot shows the vibrational progressions in CH₃O where m equals the number of quanta of excitation into the Fermi multiplet $(\nu_2 + \nu_3)^m$. For these plots the energy and lifetimes of the Fermi multiplets were averaged to produce the points on the plots. The other plots show the corresponding vibrational progressions for CD₃O, CF₃S and CH₃S radicals where n equals the number of quanta of excitation into 3^n

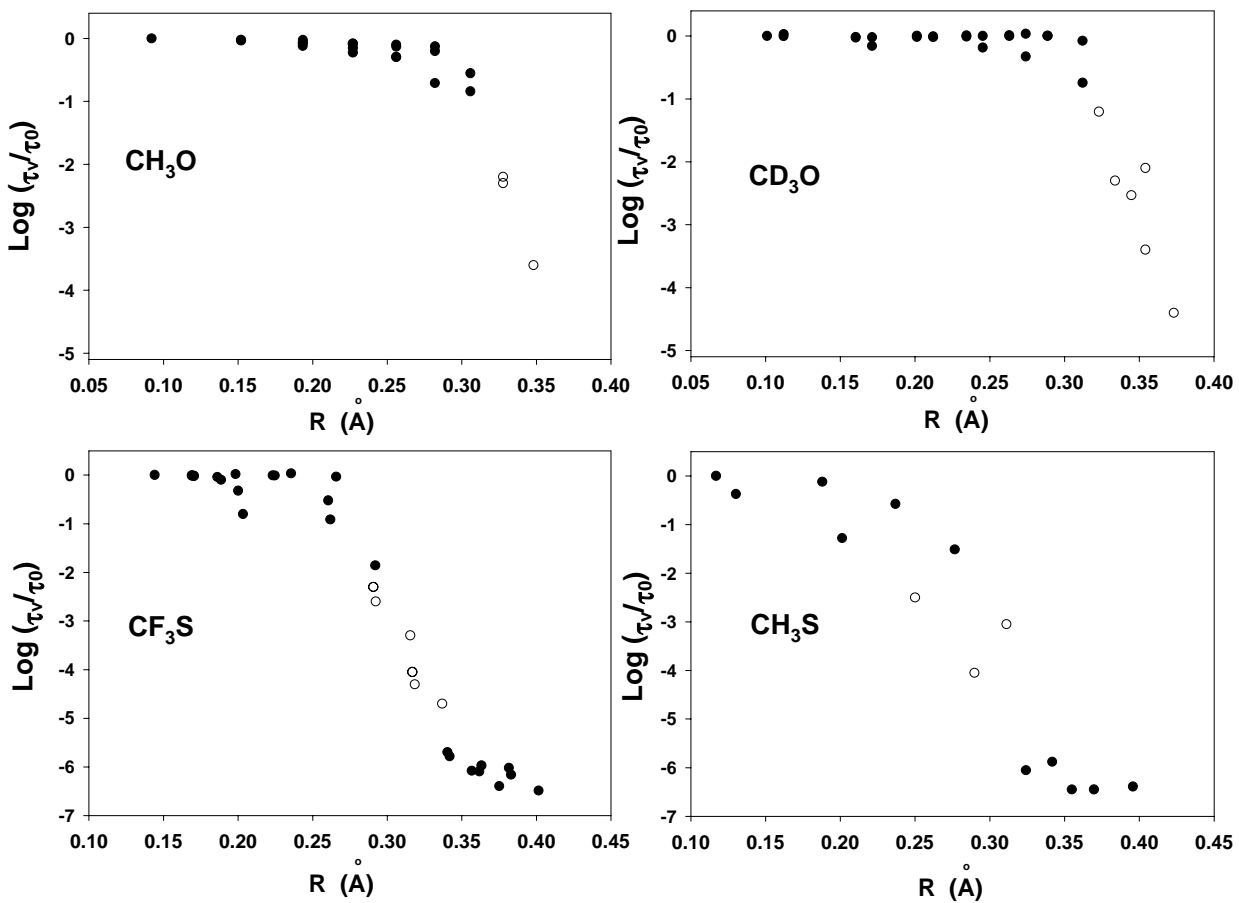


FIG. 3. Plots of the Log of the Effective Quantum Yield vs. R (R is the maximum C-O(S) extension – see text for details).

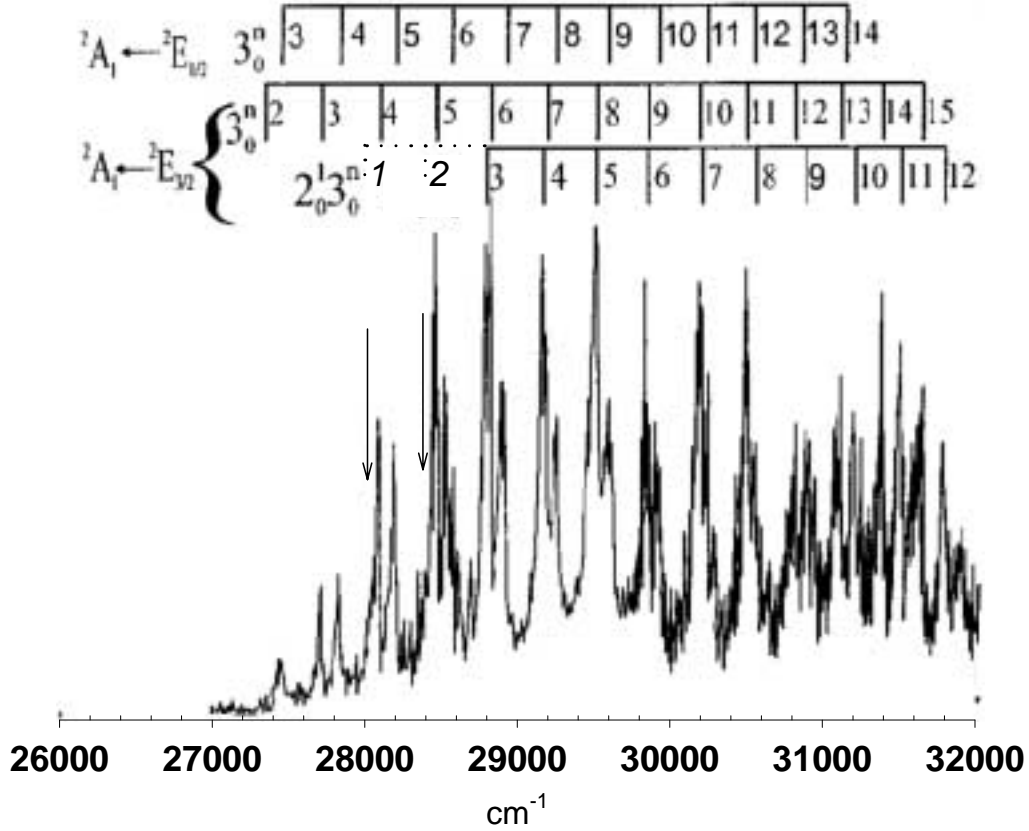


FIG. 4. Action spectrum of CH₃S adapted from Bise, *et al.*³⁵ monitoring the channel S+CH₃. The two vertical arrows point at the positions of the 2¹3¹ and 2¹3² bands, not observed in the action spectrum, but observed respectively in LIF with a significantly shortened lifetime, and in the FDS spectrum.

TABLES

TABLE I. Vibrational Frequencies, Assignments and Lifetimes for the \tilde{A} state of the CH_3S

Radical	relative frequency (cm^{-1})	technique	assignment	lifetimes		
				Chiang & Lee ³⁷	this work	Bise <i>et al.</i> ³⁵
	0	L	0_0^0	1130(70)	1090(55)ns	-
	401	L	3^1	860(30)	870(40)ns	-
	795	L	3^2	250(20)	300(30)ns	-
	1098	L	2^1	480(30)	460(30)ns	-
	1181	L	3^3	72(30)	≤ 35 ns	-
	1490	L	$2^1 3^1$	85(15)	60(20)ns	-
	1560	D	3^4	-	10ps $< \tau < 10$ ns	25ps
	1879	D	$2^1 3^2$	-	10ps $< \tau < 10$ ns	-
	1930	D	3^5	-	1.5(3)ps	10ps
	2257	D	$2^1 3^3$	-	10ps $< \tau < 10$ ns	25ps
	2291	D	3^6	-	0.4(1)ps	4ps
	2624	D	$2^1 3^4$	-	1.0(2)ps	8ps
	2624	D	3^7	-	0.5(1)ps	2ps
	2979	D	$2^1 3^5$	-	0.4(1)ps	-

TABLE II. *Ab-initio* C-O(S) Bond Length Displacements (\AA) in the Vibrationless Level of the Totally Symmetric Normal Modes in the \tilde{A} Electronically Excited State of the Methoxy Family of Radicals.

Radical	ν_1	ν_2	ν_3
CH ₃ O	0.003	0.007	0.082
CD ₃ O	0.005	0.015	0.081
CF ₃ S	0.034	0.036	0.074
CH ₃ S	0.002	0.018	0.097